Chapter 1

Analysis of Candidate Waveforms for 5G Cellular Systems

Ayesha Ijaz, Lei Zhang, Pei Xiao and Rahim Tafazolli

Additional information is available at the end of the chapter

http://dx.doi.org/10.5772/66051

Abstract

Choice of a suitable waveform is a key factor in the design of 5G physical layer. New waveform/s must be capable of supporting a greater density of users, higher data throughput and should provide more efficient utilization of available spectrum to support 5G vision of "everything everywhere and always connected" with "perception of infinite capacity". Although orthogonal frequency division multiplexing (OFDM) has been adopted as the transmission waveform in wired and wireless systems for years, it has several limitations that make it unsuitable for use in future 5G air interface. In this chapter, we investigate and analyse alternative waveforms that are promising candidate solutions to address the challenges of diverse applications and scenarios in 5G.

Keywords: waveform modulation, 5G requirements, orthogonal frequency division multiplexing, universal filtered multicarrier, generalized frequency division multiplexing, filterbank multicarrier, windowed orthogonal frequency division multiplexing, filtered orthogonal frequency division multiplexing

1. Introduction

Orthogonal frequency division multiplexing (OFDM), which uses a square window in time domain allowing a very efficient implementation, has been adopted as the air interface in several wireless communication standards, including third generation partnership (3GPP) long-term evolution (LTE) and IEEE 802.11 standard families due to the associated advantages such as:

- "Robustness against multipath fading
- Ease of implementation

- Efficient one-tap frequency domain equalization enabled by the use of cyclic prefix (CP)
- Straightforward and simple extension to very large multiple-input multiple-output (MIMO) and high gain beam forming solutions" [1]

Despite its advantages, OFDM suffers from a number of drawbacks including high peak-to-average power ratio (PAPR) and high side lobes in frequency. OFDM requires stringent time synchronization to maintain the orthogonality between different user equipments (UEs). Therefore, signalling overhead increases with the number of UEs in an OFDM-based system. Moreover, it has high sensitivity to carrier frequency offset (CFO) mismatch between different devices. All these drawbacks hinder the adoption of OFDM in the 5G air interface [1] to achieve the following key characteristics currently envisioned for 5G wireless networks:

- 1000 × higher mobile data volume per geographical area
- 10–100 × more connected devices
- 10–100 × higher typical user data rate
- 10 × lower energy consumption
- End-to-end latency of <1 ms
- Ubiquitous 5G access including in low density areas

These fundamental characteristic are envisioned based on following scenarios specified by the 5G research community [2, 3]:

1. **Bitpipe communication:** Broadcasting dense content (such as 3D or 4k video) in small-sized densely deployed cells demands several tens of Mbps to achieve a good quality of experience (QoE). An increased bandwidth and a physical (PHY) layer with high spectrum efficiency is required in this scenario. Therefore, the 5G network must rely on advanced digital communication techniques including MIMO for diversity and multiplexing, massive MIMO to improve the system spectrum efficiency, higher order modulation and efficient coding schemes, adaptive small cell clustering, multicell cooperative transmission, inter-cell interference management and efficient spectrum allocation with cognitive radios (CR).
2. **Internet of things (IoT):** This scenario targets sensory and data collecting use cases such as smart grid, health and environmental measurements and monitoring, transportation, etc. This scenario is mainly characterized by small data packets and massive connections of devices with limited power source. It does not require large channel bandwidth, and duty cycle is generally low while power saving is mandatory. The IoT devices must be able to achieve reliable communication with a loose synchronization or even asynchronous for higher energy efficiency.
3. **Tactile internet:** This scenario focuses on special applications and use cases of IoT and vertical industries with real-time constraints such as internet of vehicles (IoV) and industrial control. These new applications require very low end-to-end latency (ms-level) and high reliability (nearly 100%). The air interface and network forwarding delays need to be

reduced significantly to achieve the sub-millisecond latency requirement. Therefore, shorter frame length with minimal or no overhead, multiple access technologies which can enable grant-free transmission, and solutions for reducing network forwarding delays must be adopted. Technologies such as advanced coding and space/time/frequency diversity must be utilized for reliable data transmission.

4. **Wireless regional area network (WRAN):** This scenario focuses on coverage of low populated remote areas which suffer from low data rates and unreliable solutions. While wired technologies have limited coverage, current wireless networks operating in licensed frequencies have relatively small cell sizes which make them economically unfeasible in sparsely populated areas. The 5G networks must address large coverage areas using dynamic using dynamic channel allocation based on CR with low out of band emission (OBE) and efficiently deal with the multipath effects by reducing the impact of the CP in the overall data rate [2].

The requirements of different scenarios can be impacted by the choice of waveforms. Therefore, to address the drawbacks of OFDM and enable the aforementioned characteristics, different physical-layer waveforms are being investigated for 5G networks. The waveforms currently under consideration include filtered orthogonal frequency division multiplexing (FOFDM) [4], windowed orthogonal frequency division multiplexing (WOFDM) [5], filterbank multicarrier (FBMC) [6], generalized frequency division multiplexing (GFDM) [7] and universal filtered multicarrier (UFMC) [2]. These waveforms are being investigated to analyse their impacts on the following fundamental requirements of 5G [8]:

- Capabilities for supporting massive capacity and massive connectivity
- Support for an increasingly diverse set of services, application and users—all with extremely diverse requirements, e.g. efficient support for short-burst transmissions, IoT and massive machine type communications (mMTC)
- Flexible and efficient use of all available non-contiguous spectrum for wildly different network deployment scenarios

In this chapter, we analyse performance of alternative waveforms in terms of OBE, bit error rate (BER), time and frequency efficiency, PAPR, computational complexity and sensitivity to CFO and time offset (TO). This comparison will help determine the suitability of the candidate waveforms in different scenarios for 5G networks.

2. Candidate waveforms

2.1. Filtered orthogonal frequency division multiplexing

Large OBE, due to the rectangular shaping of the temporal signal, is one of the main shortcomings of the OFDM used in LTE. **Figure 1** shows the power spectral density (PSD) function of an OFDM waveform with carrier spacing set to 15 kHz, FFT size of 1024 and 72 samples long CP. We can observe loss of spectral efficiency due to the partial use of available bandwidth to fit in an 8 MHz emission spectrum mask (ESM).

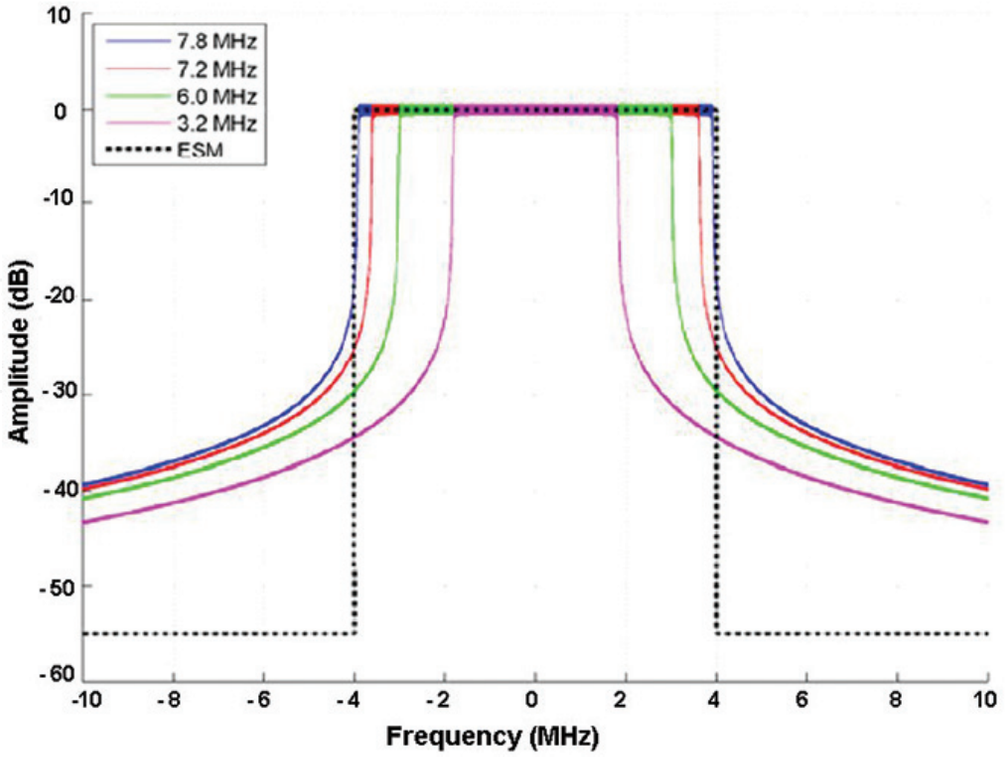

Figure 1. Power spectral density of CP-OFDM centred on the active carrier [9].

The problem of large OBE is alleviated in FOFDM using transmit filter cascaded after the modulator as shown in **Figure 2**. At the transmitter, the information bit sequence is encoded into a coded bit sequence which goes through interleaver (Π) and is mapped into QPSK/QAM symbols. Then, serial to parallel (S/P) conversion takes place and a set of N symbols are mapped onto orthogonal subcarriers using inverse fast Fourier transform (IFFT). The output from IFFT block is converted into serial data followed by CP insertion. In order to provide robustness against inter-symbol interference (ISI) and inter-carrier interference (ICI), the length of the CP must be longer than the channel impulse response. The OFDM signal is filtered by a transmit pulse shaping filter (TX filter) before transmission over the multipath fading channel. At the receiver, a receive pulse shaping filter (RX filter) is used and the signal is converted back to the frequency domain using fast Fourier transform (FFT) operation after CP removal. This is followed by one-tap equalization (the equalizer is labelled as equation in **Figure 2**) to mitigate the channel effect. The equalized signal is fed to a soft demapper, and its output is subsequently de-interleaved (Π^{-1}) and decoded to recover the information bearing signal [4].

Suitably designed filters can suppress the large side lobes of OFDM making FOFDM more bandwidth efficient while preserving the orthogonality among subcarriers. In this document, we have used a square root raised cosine (SRRC) filter, with roll-off factor $\alpha = 0.3$ truncated to 3 symbol interval ($T_r = 3T$ where T is the symbol duration) on each side of the peak at the transmitter, and the receiver filter is matched to the transmit filter. Time and frequency domain

http://dx.doi.org/10.5772/66051

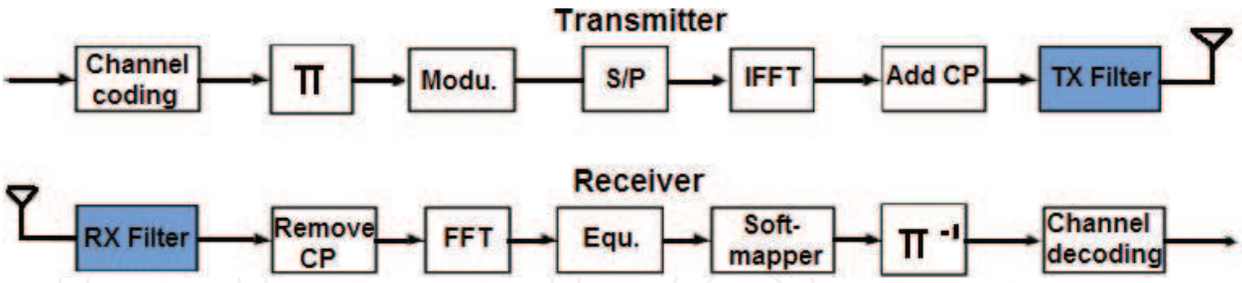

Figure 2. Transmitter and receiver structure of FOFDM [4].

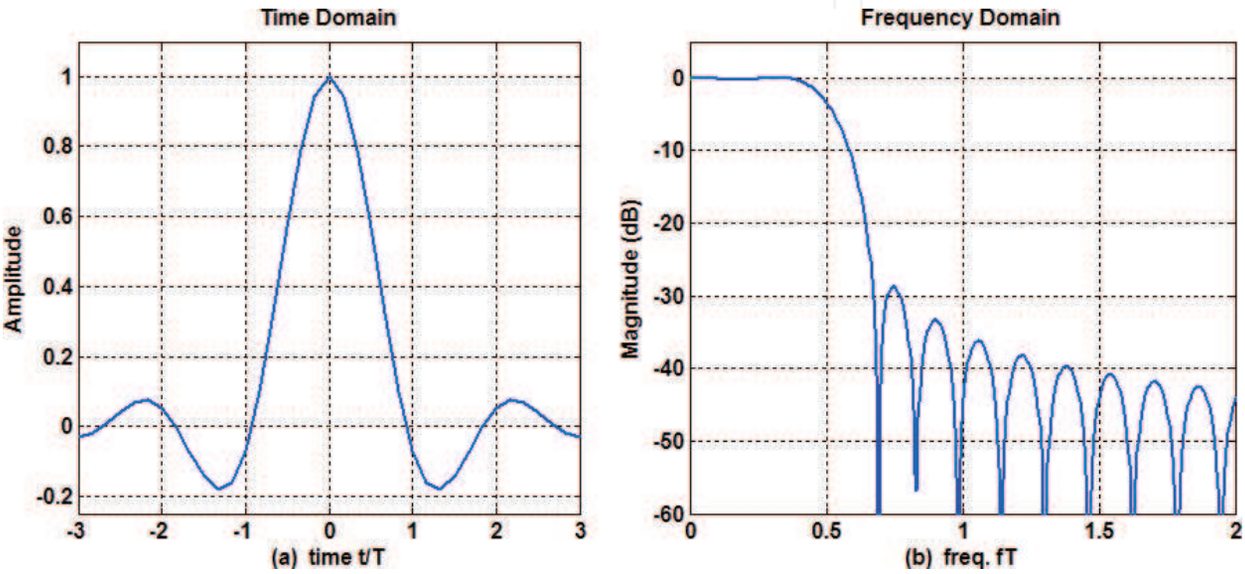

Figure 3. SRRC filter characteristics (a) time domain: the x-axis is normalized to the symbol interval T, the pulse is normalized to a peak value of unity (b) frequency domain: the frequency axis is normalized to the symbol rate $1/T$, the magnitude of the spectra, normalized to peak value of unity, is plotted in dB scale.

characteristics of such a filter are shown in **Figure 3** wherein x-axis for time and frequency is normalized to symbol interval T and symbol rate $^1/_T$, respectively.

Although FOFDM shows better spectral containment as compared to OFDM, however, when available spectrum fragments are not contiguous, filtering becomes challenging since a separate filter needs to be dynamically designed for each available chunk of spectrum.

2.2. Windowed orthogonal frequency division multiplexing

Windowed OFDM is similar to conventional OFDM, however, it uses a non-rectangular transmit window smoothing the edges of the rectangular pulse to provide better spectral containment and reduce ACI. Eq. (**1**) shows such a pulse shape in which roll-off portions are of a raised cosine shape

$$p[n] = \begin{cases} \mathbf{0.5}\left(\mathbf{1} + \boldsymbol{cos}\left\{\{\pi\left(1 + \dfrac{\boldsymbol{n}}{\boldsymbol{\beta N_T}}\right)\right\}\right), & 0 \leq \boldsymbol{n} < \boldsymbol{\beta N_T} \\ 1, & \boldsymbol{\beta N_T} \leq \boldsymbol{n} < \boldsymbol{N_T} \\ 0.5\left(1 + \boldsymbol{cos}\left\{\pi \dfrac{\boldsymbol{n} - \boldsymbol{N_T}}{\boldsymbol{\beta N_T}}\right\}\right), & \boldsymbol{N_T} \leq \boldsymbol{n} \leq (\boldsymbol{\beta} + 1)\boldsymbol{N_T} - 1 \end{cases} \quad (1)$$

In Eq. (**1**), $0 \leq \beta$ 1, is the roll-off factor which controls the length of the roll-off portion of the non-rectangular window, i.e. $\beta(N + N_{CP})$, where N_{CP} is the length of CP in samples. Due to multiplication of CP with a non-unity function, orthogonality will be in general lost in a multipath channel. In order to preserve orthogonality, an extended CP is used in WOFDM and the original samples of the CP are kept outside the roll-off part of the windowing function. Improved PSD side lobe decay in WOFDM can save the guard band overhead of the current OFDM deployments, e.g. 10% overhead in LTE. However, the use of extended CP in WOFDM reduces its spectral efficiency as compared to OFDM. Therefore, both frequency and time domain overheads need to be taken into account to determine overall improvement in spectral efficiency as compared to OFDM. WOFDM also uses a cyclic suffix (CS) after each data block in addition to the CP before each data block. The spectral loss due to additional overhead of CS is partly compensated by overlapping the CP and CS of consecutive symbols.

2.3. Filter bank multicarrier

Filter bank multicarrier applies filtering on a per-subcarrier basis and is considered as an attractive alternative to OFDM to provide improved out-of-band spectrum characteristics. Since subcarrier filters are narrow in frequency and thus require long filter lengths (normally at least $4T$ to preserve an acceptable ISI and ICI), the symbols are overlapping in time. To comply with the real orthogonality principle, offset-QAM (OQAM) can be applied and, therefore, FBMC is not orthogonal in the complex domain. The most common FBMC technique is the FBMC/OQAM, which is also known as OFDM with offset quadrature amplitude modulation (OFDM/OQAM) [10].

In FBMC, the prototype filter needs to be carefully designed to minimize or eliminate ISI and ICI while keeping the side lobes small. These prototype filters are implemented using an efficient technique called polyphase implementation, which uses multi-rate signal processing techniques to reduce the complexity by joint implementation of all synthesis or analysis filters in the filter bank. The transmitted signal in FBMC is the sum of the outputs of a bank of N filters, whose length is given by $L = N \times p$, where N is the FFT size and p is the length of each polyphase filter. We have used an isotropic orthogonal transform algorithm (IOTA) prototype function with $p = 6$, for use in FBMC system, which is well-localized in time and frequency domain as shown in **Figure 4**.

Since subcarriers can be better localized in FBMC due to more advanced prototype filter design, therefore the CP can be removed resulting in improved spectral efficiency as compared to OFDM. This is in addition to the spectral efficiency gain due to reduced guard band in FBMC. However, FBMC/OQAM incurs an overhead due to transition times (tails) at both ends

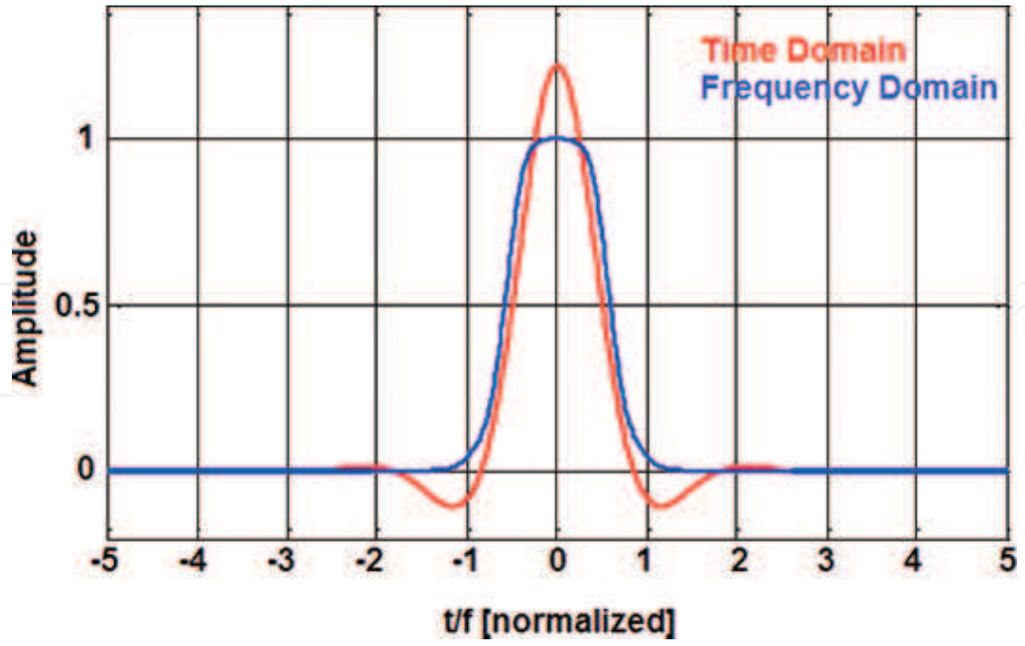

Figure 4. Time and frequency response of IOTA prototype function. Time domain pulse is normalized to average power of unity. The *x*-axis is normalized to the symbol interval *T*, the frequency axis for spectra is normalized to the symbol rate $1/T$ and the frequency domain spectrum is normalized to peak value of unity.

of a transmission burst and an overhead due to the $T/2$ time offset between the OQAM symbols [11] (total tail duration is equal to length of the prototype filter). Although solutions have been proposed to remove signal tails of OFDM/OQAM signals [11], however, the overhead cannot be removed totally, without increasing its sensitivity to time and frequency misalignments, and it increases the latency of communication.

2.4. Universal filtered multicarrier

As the name implies, UFMC is also a filtered multicarrier modulation scheme using suitably designed filters to reduce OBE like FOFDM and FBMC and combines the benefits of the two schemes. UFMC applies filtering to chunks of contiguous subcarriers instead of single subcarriers (as in FBMC) or the complete band (as in FOFDM). **Figure 5** shows the block diagram of a UFMC transmitter with total bandwidth divided into B sub-bands where the time-domain transmit vector x for a particular multicarrier symbol is the superposition of the sub-band-wise filtered components, with filter length L and FFT length N. The transmit signal can be mathematically described as follows:

$$x = \sum_{i=1}^{B} F_i V_i s_i \tag{2}$$

where S_i is the transmit vector containing n_i complex QAM symbols for transmission in ith sub-band. For each of B sub-band, indexed i, S_i is transformed to time-domain by the IDFT-matrix V_i with dimensions $[N \times n_i]$. N is the required number of samples per symbol to

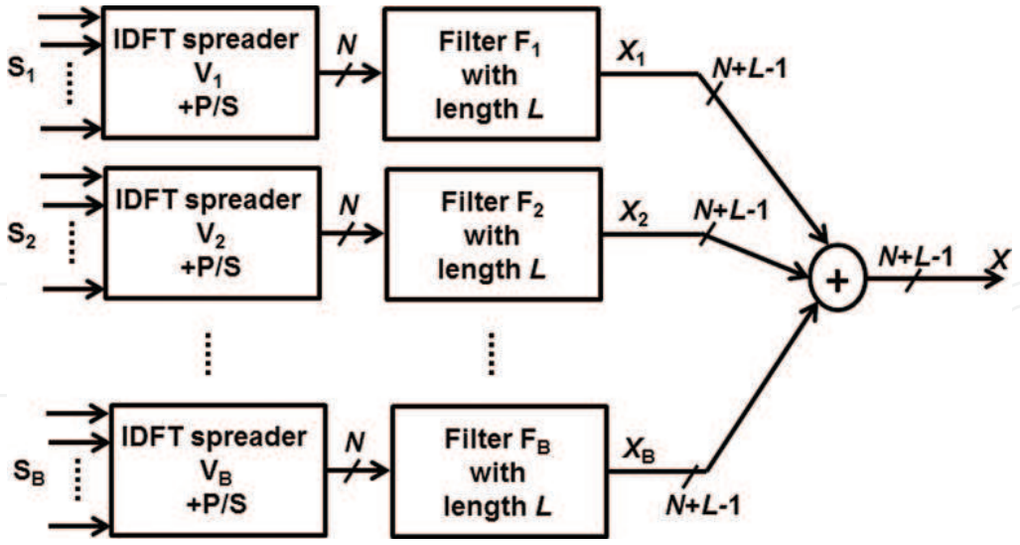

Figure 5. UFMC transmitter.

represent all sub-bands without introducing aliasing (i.e. N depends on the overall covered bandwidth). "V_i includes the relevant columns of the inverse Fourier matrix according to the respective sub-band position within the overall available frequency range. F_i is a Toeplitz matrix with dimensions $[(N + L - 1) \times N]$, composed of the filter impulse response, performing linear convolution" [2]. Unlike OFDM, CP can be dropped in UFMC and its additional symbol duration overhead is used to introduce sub-band filters. Since filtering is applied to a sub-band, these filters can be shorter [2] (UFMC filters are in the order of an OFDM CP) than the per-subcarrier filters of an FBMC system improving the suitability of UFMC for communicating in short bursts, compared to FBMC. Moreover, orthogonality is still maintained between subcarriers. Since the same filter can be used for each sub-band, spectral holes can be dynamically utilized without posing a challenge in implementation as compared to FOFDM.

We have used Dolph-Chebyshev filters with side-lobe-attenuation equal to 40 dB and filter length L equal to one sample larger than the CP length in an LTE system. **Figure 6** depicts the impulse and frequency response for an exemplary setting with $L = 73$ and $N = 1024$.

Since UFMC modulates each data symbol at the same time and the same frequency as in OFDM, its receiver [2] can demodulate legacy OFDM signals and UFMC modulated signal can be directly demodulated by the legacy OFDM receiver. This feature makes UFMC-based system backwards compatible with the legacy OFDM systems [12]; a feature missing in FBMC.

2.5. Generalized frequency division multiplexing

GFDM is a block-based, non-orthogonal multicarrier transmission scheme capable to spread data across a two-dimensional (time and frequency) block structure (multi-symbols per multicarriers). The block-based transmission in GFDM is enabled by circular pulse shaping of the individual subcarriers. "The main difference between OFDM and GFDM is that the latter

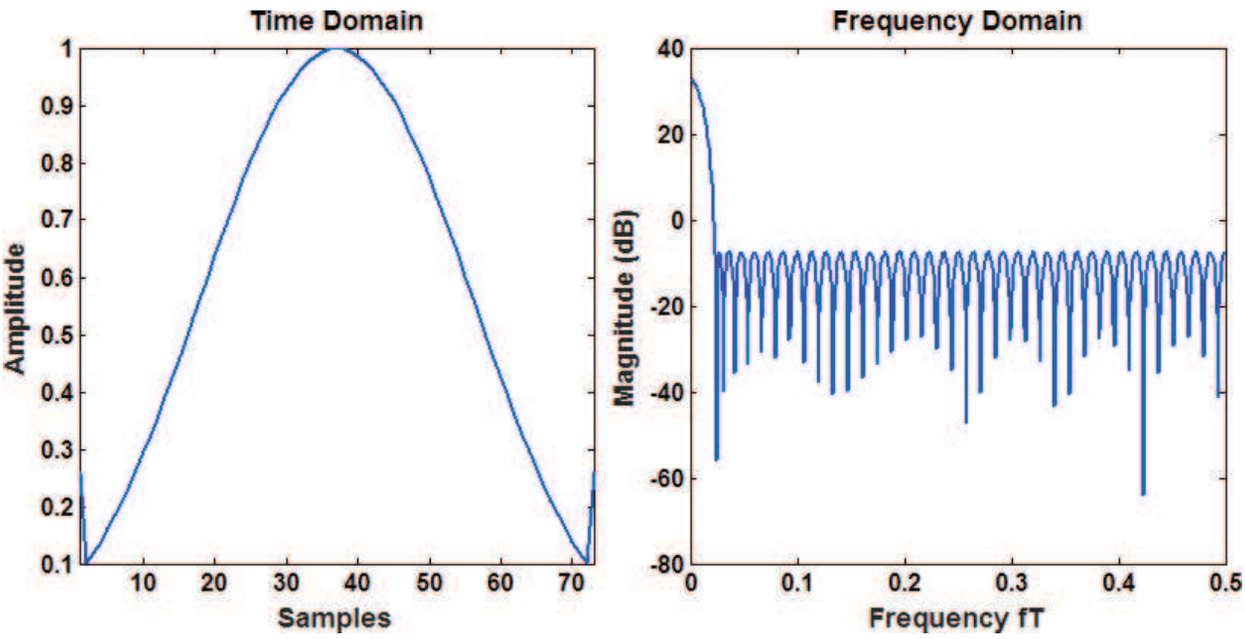

Figure 6. Chebyshev filter characteristics in time and frequency domain. The time domain pulse is normalized to a peak value of unity. The frequency axis is normalized to the symbol rate 1/*T*.

transmits *MN* data symbols per frame using *M*time slots with *N*subcarriers where each data symbol is represented by a pulse shape $g(t)$, whereas OFDM transmits *N* data symbols using one time slot with *N* subcarriers, where each symbol is filtered by a rectangular pulse shape" [2]. GFDM cannot only model the spectrum shape by choosing an appropriate pulse shape to provide a very low OBE, frequency spacing between subcarriers is also more flexible in GFDM than in OFDM which allows for a higher flexibility for spectrum fragmentation. GFDM can achieve higher spectral efficiency since it does not need guard band to avoid adjacent channel interference (ACI).

The baseband block diagram of a GFDM transceiver system is given in **Figure 7**. The data symbols to be transmitted on *i*th subcarrier, $d_i = d_i(0), \ldots, d_i(M-1)]^T$, are first up-sampled by the factor of *N* to form an impulse train $s_i(n) = \Sigma_{m=0}^{M-1} d_i(m)\delta(n-mN), n = 0, \ldots, NM-1$. This signal is then circularly convolved with the prototype filter and up-converted to its corresponding subcarrier frequency. The resulting signals for all subcarriers are summed up to form the GFDM symbol $x(n)$ given below:

$$x(n) = \sum_{i=0}^{N-1} \sum_{m=0}^{M-1} d_i(m) g_{\{(n-mN) \bmod MN\}} e^{j\frac{2\pi in}{N}}, \; n = 0, \ldots, NM-1 \tag{3}$$

where g_l is the *l*th coefficient of the prototype filter. Circular filtering helps to remove the latency associated with the prototype filter transient intervals when conventional linear convolution is used like in the FBMC schemes. We have used an SRRC filter with roll-off factor $\alpha = 0.3$ in the GFDM-based link level simulator. The impulse response and frequency domain characteristics for the prototype filter are given in **Figure 8** for $N = 128$ and $M = 7$.

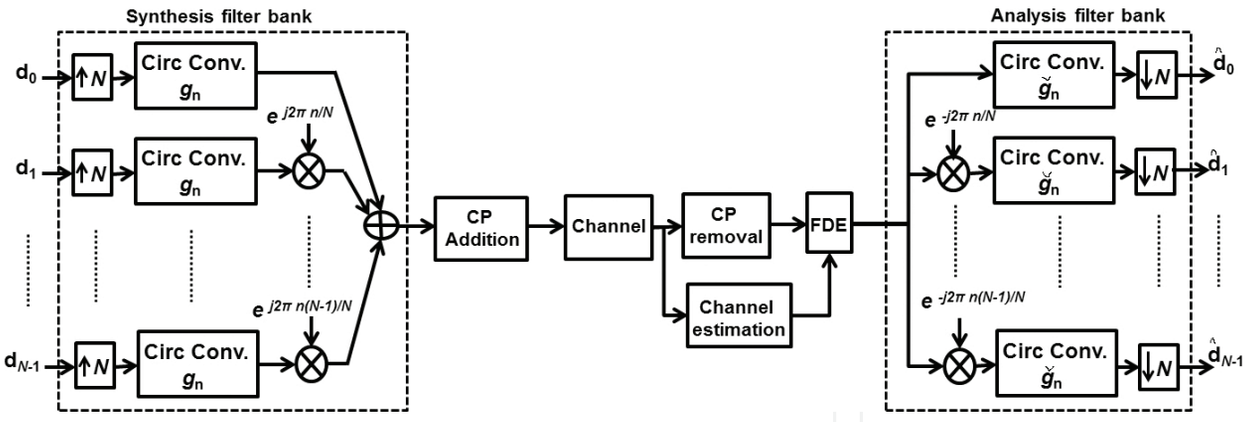

Figure 7. Block diagram of a GFDM transceiver system [7].

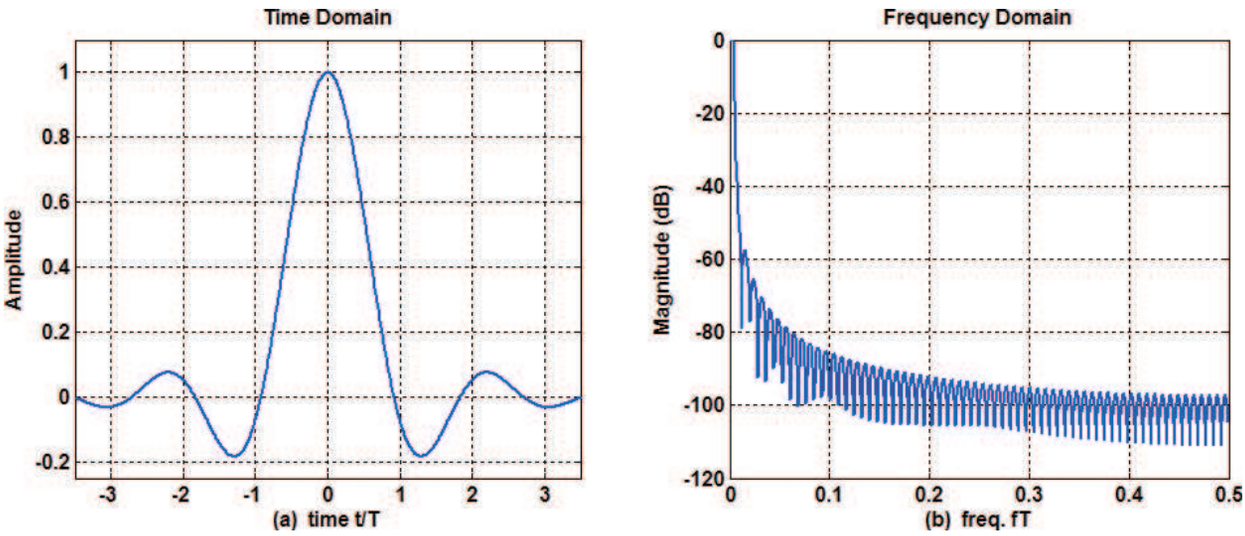

Figure 8. Time and frequency domain characteristics of an SRRC filter in GFDM transmitter (a) time domain: the x-axis is normalized to the symbol interval T, the pulse is normalized to a peak value of unity (b) frequency domain: the frequency axis is normalized to the symbol rate $1/T$, the magnitude of the spectra, normalized to peak value of unity, is plotted in dB scale.

Based on Eq. (**3**), GFDM signal $\boldsymbol{x} = [x(0), \ldots, x(MN-1)]^T$ can also be formulated as $\boldsymbol{x} = \boldsymbol{Ad}$ where $\boldsymbol{A}$ is an $MN \times MN$ modulation matrix whose elements can be represented as:

$$[A]_{nm} = g_{\{(n-mN) \bmod MN\}} e^{j\frac{2\pi nm}{NM}} \tag{4}$$

Lastly, on the transmitter side, a cyclic prefix of N_{CP} samples is added to the GFDM data block to produce $\tilde{\boldsymbol{x}}$. Since it uses only one CP for M time slots (i.e. one block) rather than a CP for each slot (i.e. multicarrier symbol) as is the case in OFDM, it has higher spectral efficiency than the latter. GFDM turns into OFDM when $M = 1$ and $\boldsymbol{A}$ is an $N \times N$ inverse Fourier matrix. In CP-based GFDM systems, frequency domain equalization (FDE) can be performed after CP removal to compensate for the multipath channel impairments. The received signal, after channel equalization, can be demodulated after using linear receivers such as zero forcing

(ZF), matched filter (MF) and minimum mean square error (MMSE) receivers. While MF receiver maximizes signal-to-noise ratio (SNR) per subcarrier, it cannot completely remove ICI. Self-interference due to non-orthogonality of the neighbouring subcarriers and time slots can be removed using ZF receiver at the expense of noise enhancement. MMSE receiver can be used to make a trade-off between self-interference and noise enhancement [2].

3. Comparison of waveforms

Now, we present simulation results and discuss performance of the candidate waveforms. Based on the characteristics of these waveforms, we discuss their suitability for the scenarios which are being foreseen for 5G networks. The simulation parameters are given in **Table 1**.

3.1. Power spectrum

Figure 9 shows power spectral density of different waveforms assuming non-contiguous fragments of spectrum are available for transmission. In **Figure 9**, two available spectrum fragments are separated by an unavailable band while the spectrum at the two edges is also not used for transmission. It is observed that UFMC and FBMC reduce the OBE by reducing spectral leakage from the transmission subcarriers to the unused neighbouring band. Hence, these waveforms are more suitable candidates, as compared to OFDM, for applications that

Parameter	Settings			
MCM schemes	OFDM, WOFDM, FOFDM, FBMC, UFMC, GFDM			
Subcarrier spacing (Δf)	15 KHz			
Resource block size	12 subcarriers			
Sub-band size for UFMC (D)	12 subcarriers			
No. of MC symbols per subframe (M)	7			
Bandwidth	5 MHz			
FFT size (N)	512			
Encoder	Turbo coding, rate 1/3, 1			
CP length (samples) (N_{CP})	32 for OFDM, FOFDM and GFDM. 0.25 × FFT size for WOFDM. 0 for FBMC and UFDM			
Channel model	Extended pedestrian A (EPA) [13], AWGN			
Channel estimation	Ideal			
Equalizer	1-tap MMSE FDE			
Sub-frames	10,000			
Filters	FOFDM	FBMC	UFMC	GFDM
	RRC filter $\alpha = 0.3$ $L = 13$	IOTA pulse $p = 6$	Dolph-Chebyshevside lobe attenuation = 40 dB $L = 33$	RRC filter $\alpha = 0.1$

Table 1. Simulation settings.

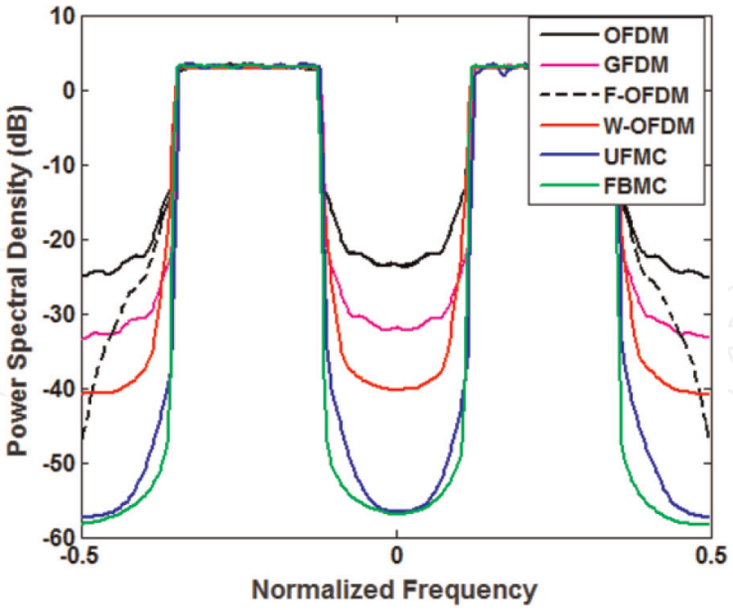

Figure 9. Power spectral density of waveforms with fragmented spectrum around the centre frequency.

have strict ACI requirements such as in cognitive radio (CR). It also implies that these waveforms will not need large guard bands to avoid ACI, thereby, improving spectral efficiency and facilitating carrier aggregation. WOFDM also shows considerably lower OBE as compared to OFDM. However, OBE of GFDM is not significantly lower than OFDM due to the abrupt changes of the signal value between GFDM blocks.

Although FOFDM has lower side lobes as compared to OFDM in the two unused bands at the edges, its OBE to the unavailable band between the available fragments is the same as that of OFDM. This is due to the use of filter over the whole band in FOFDM using OFDM as the underlying technology. Therefore, FOFDM cannot efficiently utilize non-contiguous chunks of spectrum.

3.2. Bit error rate performance

Having analysed the PSD properties of transmitted signal using different MCM schemes, we now analyse the BER performance of different waveforms assuming only one transmitter and receiver using the entire bandwidth for data transmission and no interferer in adjacent frequency bands. We first simulate the BER performance in an AWGN only channel using the QPSK (OQPSK for FBMC) modulation without error correction coding. Then BER performance was simulated using a rate 1/3 turbo code in the extended pedestrian A (EPA) channel [13] assuming perfect channel knowledge to analyse the performance of different waveforms in frequency selective channel. The results were obtained by averaging BER over 10,000 subframes transmitting 7 MC symbols per subframe. For FBMC, we used hard truncation by discarding two FFT blocks on both sides of the transmit matrix to reduce the overhead caused by filter tails. Similarly, hard truncation was employed to completely remove filter tails in FOFDM. Although CP is not needed for OFDM, GFDM, FOFDM in the AWGN channel, it is

still used here to comply with the standard system configuration. Simulation results presented in **Figure 10** show that all schemes have comparable BER performance in the AWGN channel in the absence of ACI. Slight discrepancy in the performances of different waveforms as compared to the theoretical performance is due to the overhead imposed by the CP or filter tails. WOFDM shows 1 dB degradation due to the largest overhead, i.e. 25% of FFT size. FBMC shows 0.5 dB degradation as compared to the theoretical performance of QPSK in an AWGN channel while other waveforms are very close to the theoretical curve.

Figure 10 also shows BER performance using QPSK/OQPSK with code rate = 1/3 in an EPA channel using parameters specified in **Table 1** and assuming perfect knowledge of noise variance is available for MMSE equalizer. It is observed that all waveforms, except WOFDM and FBMC, show similar performance as that of OFDM. While loss in WOFDM is due to greater CP overhead, FBMC also shows similar performance as that of WOFDM in multipath fading channel under consideration.

3.3. Time-frequency efficiency

Time-frequency efficiency r_{TF} which depends on the characteristics of the underlying waveform of an air interface is an important parameter to compare the performance of different waveforms. It is defined as follows [14]:

$$r_{TF} = r_T.r_F = \frac{L_D}{L_D + L_T} \times \frac{N_u}{N'} \tag{5}$$

where r_T is "the efficiency in time domain relating the information carrying body (L_D) of the burst/subframe to its overall length including the tails (L_T)" [14]. Hence, length of the cyclic prefix and the filters are of relevance for r_T. r_F is the efficiency in frequency domain, and it is the ratio of number of usable subcarriers N_u (i.e. excluding guard carriers) to the overall number of subcarriers N' within the usable band.

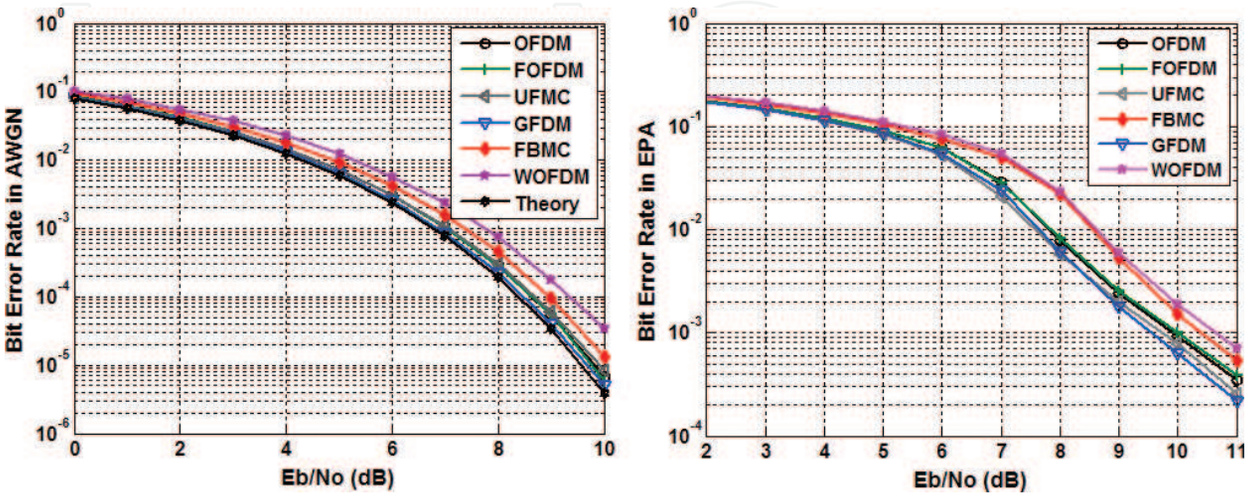

Figure 10. BER for QPSK/OQAM in AWGN (code rate = 1) and EPA (code rate = 1/3) channel.

Here, we present time domain efficiency taking into account basic signal characteristics,i.e. how many data symbols may be included into a given time-frequency block for a certain CP and filter length without reflecting on other overheads such as pilot symbols.

3.3.1. Time domain efficiency

As shown in Eq. (**5**), time domain efficiency is given by $r_T = L_D/(L_D + L_T)$. If we assume the burst to contain M multicarrier symbols (each comprising of N samples), the length of the information carrying body of the transmitted signal is $L_D = MN$. The tails of different waveforms, with design specifications given in Section 2, are given below:

$$L_{T,OFDM} = MN_{CP} \tag{6}$$

$$L_{T,F-OFDM} = MN_{CP} \tag{7}$$

$$L_{T,W-OFDM} = MN_{CP} = 0.25 \times MN \tag{8}$$

$$L_{T,FBMC} = N \tag{9}$$

$$L_{T,UFMC} = M(L-1) \tag{10}$$

$$L_{T,GFDM} = N_{CP} \tag{11}$$

Figure 11 shows time domain efficiency of candidate waveforms versus the frame/burst size ranging from 1 to 20 MC symbols per frame/burst with FFT size (N) equal to 1024 and CP length equal to 72 samples. The length of UFMC filter, i.e. $L = 73$. It can be observed from these results that FOFDM using hard truncation has similar time domain efficiency as OFDM as is also evident from Eqs. (**6**) and (**7**). Time-domain overhead for both schemes is proportional to the frame size (M) and CP length. Therefore, their time-efficiency is constant for a fixed size of CP. This is also true for WOFDM, however, it has lower efficiency than OFDM due to longer CP. GFDM has the highest efficiency due to its block-based nature using one CP per frame. FBMC, on the other hand, has significantly lower efficiency than OFDM particularly for very short burst sizes. Its performance approaches that of OFDM for the design used by LTE (indicated by black vertical line), i.e.14 MC symbols per frame outperforms OFDM for longer bursts.

3.3.2. Frequency domain efficiency

As shown in Eq. (**5**), frequency domain efficiency is given by $r_F = N_u/N'$. Using LTE as reference and assuming a transmission bandwidth of 10 MHz with subcarrier spacing 15 kHz, the number of subcarriers N' fitting into the given bandwidth is:

$$N' = \frac{10\ \text{MHz}}{15\ \text{kHz}} = 666 \tag{12}$$

According to the LTE standard, number of subcarriers actually carrying data is $N_{U,\ OFDM} = 600$. For FBMC, with very low out-of band radiation as shown in **Figure 9**, one guard subcarrier at each side of the band is sufficient and thus $N_{U,\ FBMC} = 664 - (N_g - 1)$ where N_g reflects the number of users sharing the band. Since FBMC is not orthogonal with

http://dx.doi.org/10.5772/66051

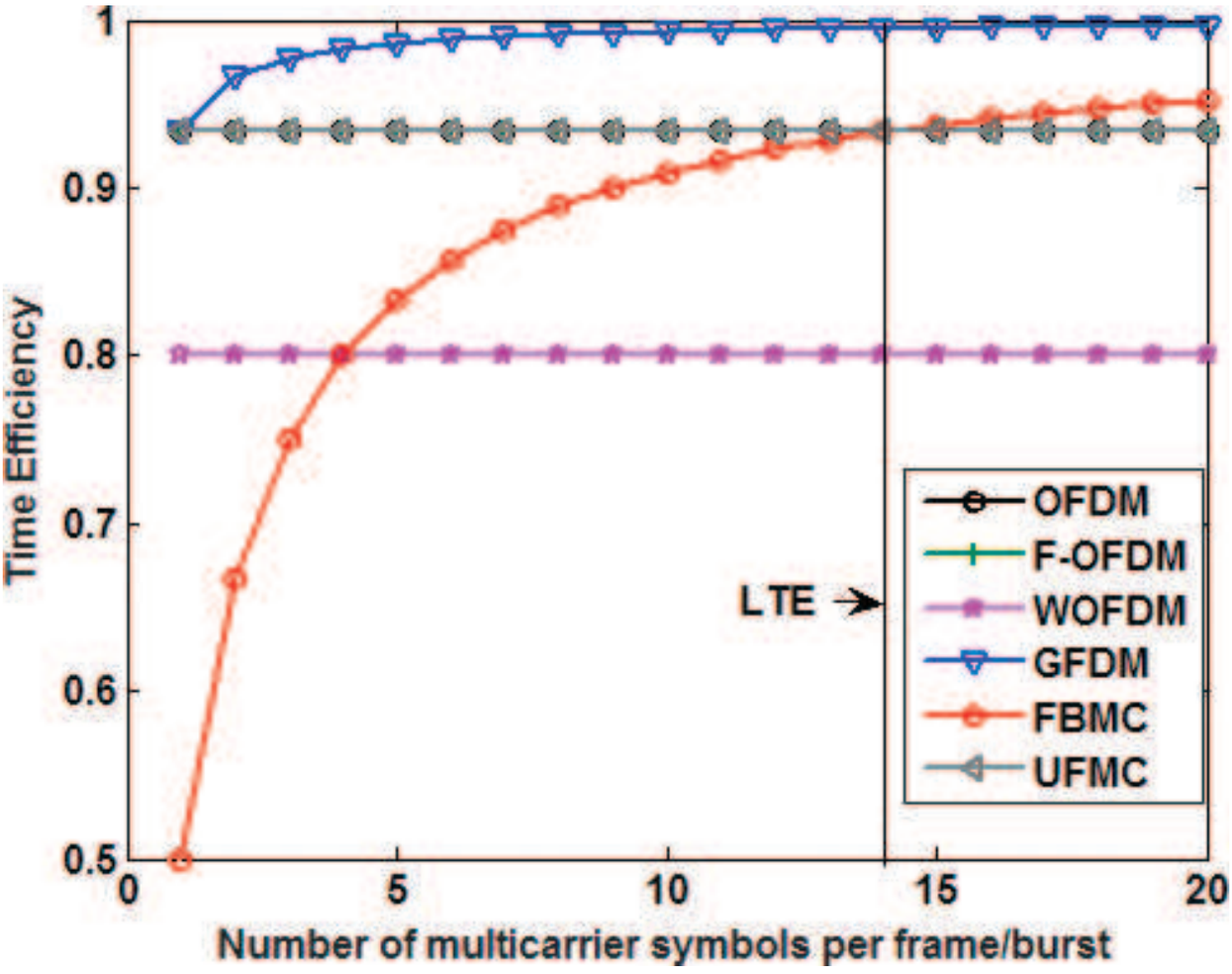

Figure 11. Time domain efficiency versus burst size.

respect to the complex plane, an additional guard subcarrier is needed to separate UL transmissions [if complex precoding is applied (the same holds for DL transmissions)] of users being allocated adjacent in frequency. "This is necessary as the transmissions of different users are experiencing different channel gains introducing multi-user interference at the allocation edges. Hence, N_g is equal to the number of users sharing the transmission time interval (assuming continuous user allocations)" [14]. Assuming a scenario where whole bandwidth is available for single user transmission, $N_{U,\ FBMC}$ = 664. GFDM, UFMC and WOFDM designed for very low OBE, as shown in **Figure 9**, also need one subcarrier guard at each side of the band. Therefore, $N_{U,\ UFMC} = N_{U,\ WOFDM} = N_{U,\ GFDM} = 664$.

Since FOFDM, with an SRRC filter design as given in Section 2.1, does not exhibit very low OBE as compared to OFDM, $N_{U,\ FOFDM}$ is expected to be quite similar to $N_{U,\ OFDM}$ and this value needs to be decided after further careful investigation of the OBE characteristics and spectral emission mask requirements in different scenarios. For the sake of analysis, we choose it arbitrarily to be equal to $N_{U,\ OFDM}$.

3.3.3. Overall time-frequency efficiency

Assuming a single user occupying the whole bandwidth, i.e. N_g = 1, **Figure 12** shows the comparison of time-frequency efficiency of different waveforms versus the number of multicarrier symbols per burst. Since frequency domain efficiency of all the waveforms except OFDM and FOFDM is nearly unity, their overall efficiencies remain unchanged. However, overall time-frequency efficiency of OFDM and FOFDM reduces by 10%. Therefore, we observe that while time-domain efficiency of UFMC design under consideration is similar to that of OFDM, its overall efficiency is better due to lower guard band required for UFMC. It can also be observed that the overall time-frequency efficiency of FBMC approaches the efficiency of OFDM when burst size approaches 5, and it exhibits greater efficiency for burst sizes exceeding 5 multicarrier symbols. Based on these analytical results, we can conclude that both UFMC and GFDM are more suitable for short burst transmissions as compared to other MCM schemes. FBMC is more suitable for long burst transmission and is inefficient for short burst communication.

3.4. Peak-to-average power ratio performance

Peak-to-average power ratio (PAPR) measures the envelope variation of a waveform and is defined as the peak amplitude of the waveform divided by its root-mean-square value. Large

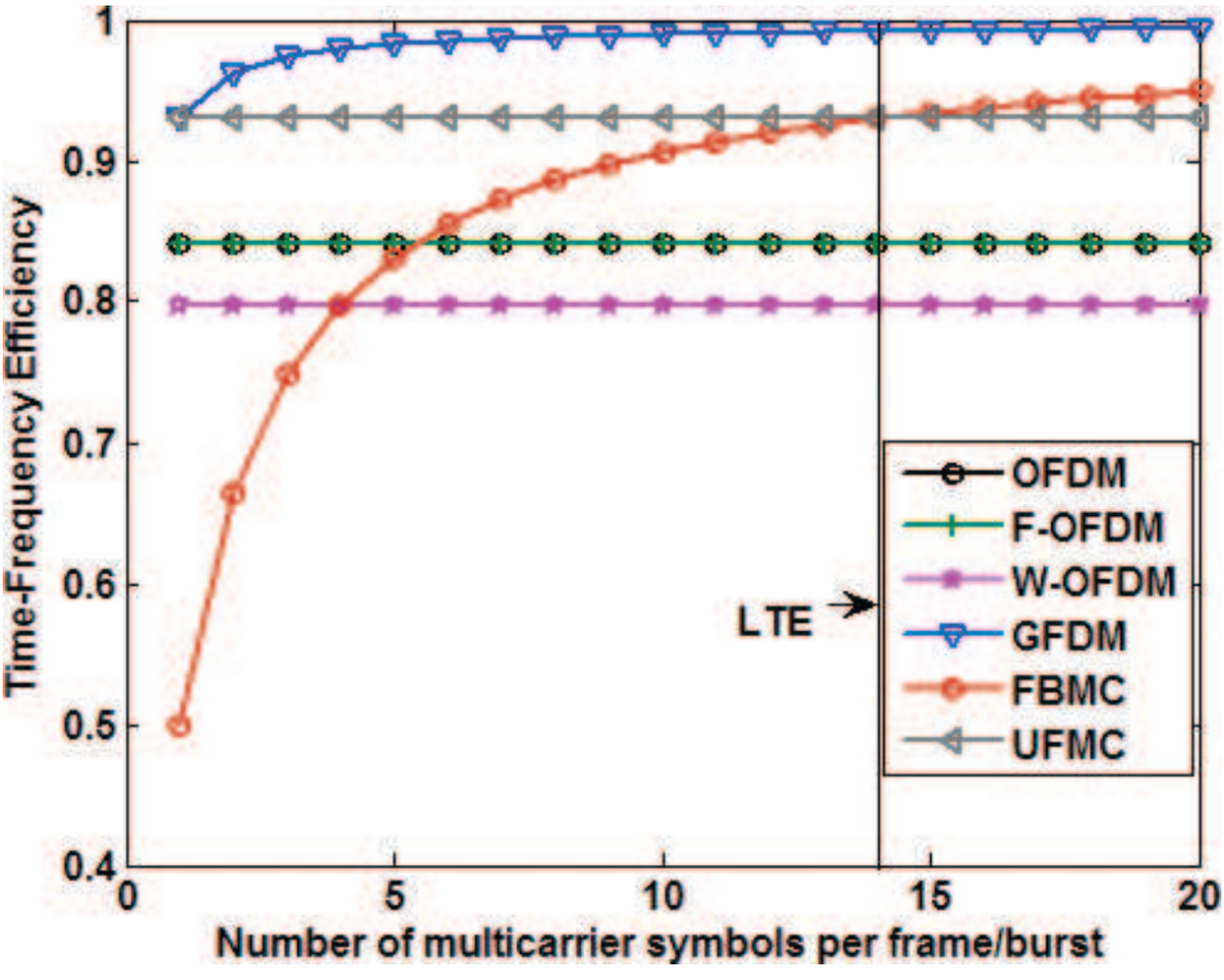

Figure 12. Time-frequency efficiency versus burst size.

http://dx.doi.org/10.5772/66051

PAPR requires power amplifiers to have a very large linear range. Otherwise, the nonlinearity leads to signal distortion, which causes spectral regrowth and higher BER. It was gathered from the literature survey [15] that all multicarrier candidate waveforms suffer from large PAPR. **Figure 13** presents the PAPR performance comparison of different waveforms and confirms the findings from the literature as it is seen that all the candidate waveforms exhibit large PAPR. Comparing the relative performance, we observe that OFDM and WOFDM have the lowest PAPR while FOFDM shows the highest PAPR. Other MCM schemes using filter to limit OBE also show higher PAPR as compared to OFDM. A general observation from these results is that use of filters in MCM schemes to limit OBE, increases the PAPR due to interference/overlapping among the time domain samples of filtered signals.

3.5. Impact of CFO

In this section, we present results of simulations carried out to analyse the impact of carrier frequency offset on the BER performance of different waveforms. Simulations were performed

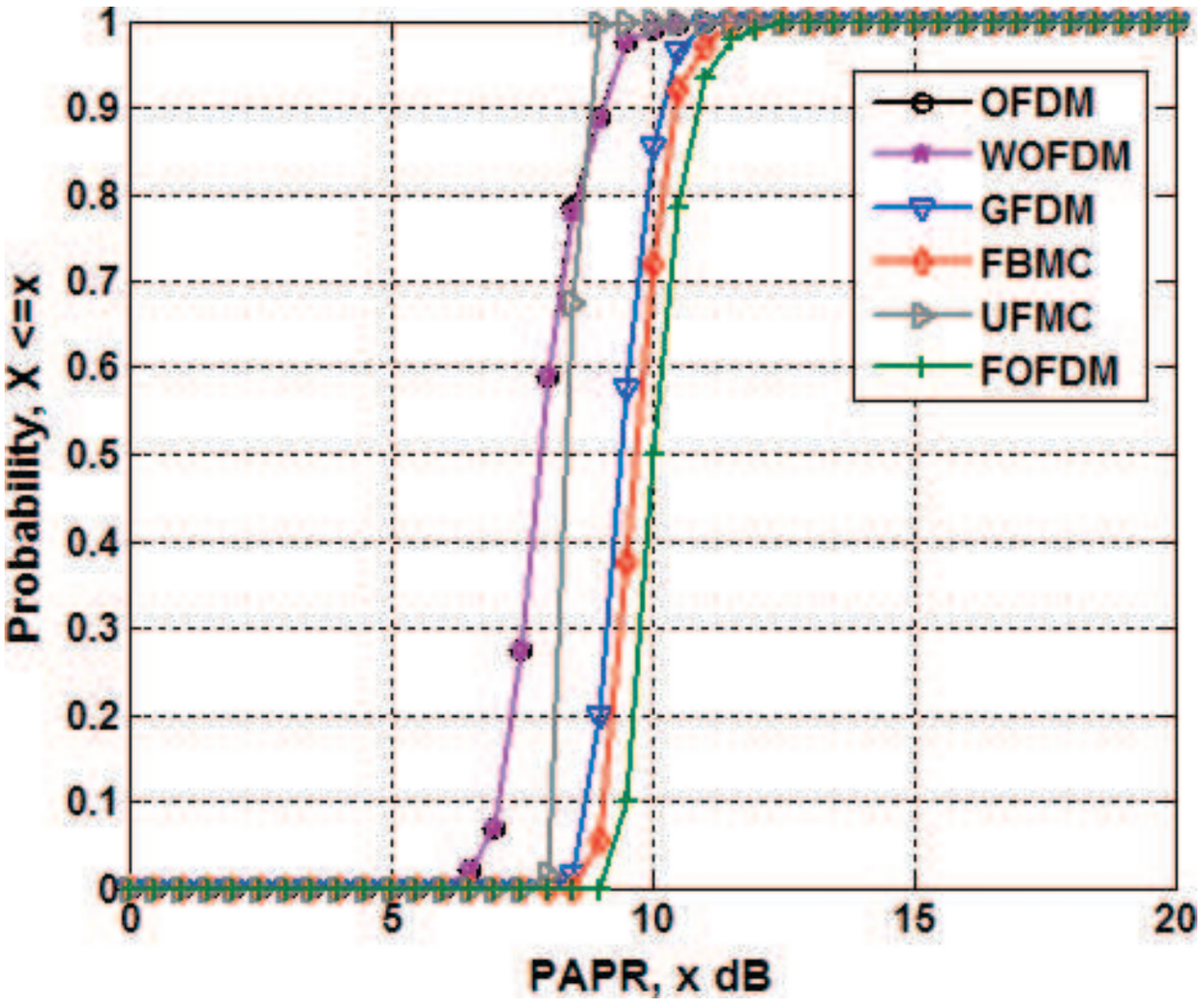

Figure 13. PAPR performance of candidate waveforms.

using parameters as given in **Table 1** for QPSK in an AWGN channel only, hence, the channel does not introduce any impairment.

Figure 14 shows the raw BER of QPSK assuming $\in$ = 0.05, 0.1, where $\in = f'T$ is the normalized CFO, i.e. the frequency offset f' normalized by the subcarrier spacing $1/T$. Note that this is the residual CFO and is not compensated for in the channel equalization block. It is observed from simulation results that all the waveforms show similar level of degradation, approximately 2 dB, in BER performance for $\in$ = 0.05 as compared to the BER performance shown in **Figure 10** for a perfectly synchronized receiver in an AWGN channel. However, the degradation in FBMC is comparatively larger, approximately 2.5 dB, as compared to other waveforms. This is due to the intrinsic interference in the FBMC scheme and the degradation becomes worse when normalized CFO increases to 0.1 due to increased level of intrinsic interference in FBMC. Comparing the results of $\in$ = 0.05 and $\in$ = 0.1, it can be seen that for larger value of CFO, all waveforms except FBMC show approximately 10.5 dB degradation and also tend to exhibit an error floor for higher values of Eb/No where inter-carrier interference becomes dominant due to larger CFO. Large degradation in the BER performance of FBMC indicates the need for intrinsic interference cancellation techniques or re-designing filters with even better localized pulse shapes to make FBMC more robust to CFO.

3.6. Impact of time offset

In this section, we present BER performance of different waveforms to analyse their sensitivity to timing offset (TO). We simulated BER performance for two different arbitrary values of TO, i.e. 80 and 150 samples in AWGN channel only. Hence, it is ensured that the channel itself does not introduce any time spreading. Simulation results given in this section were obtained by estimating channel using noise-free samples of received signal. We know from the literature survey that due to intrinsic interference in FBMC, it requires special pilot design, e.g. auxiliary

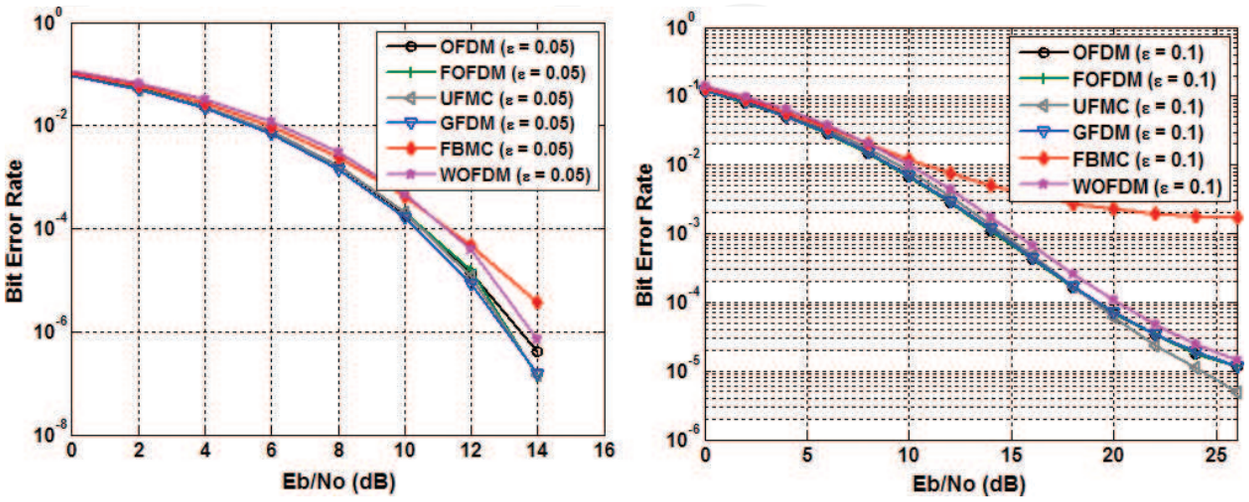

Figure 14. BER of QPSK/OQPSK in AWGN for ϵ = 0.05, 0.1.

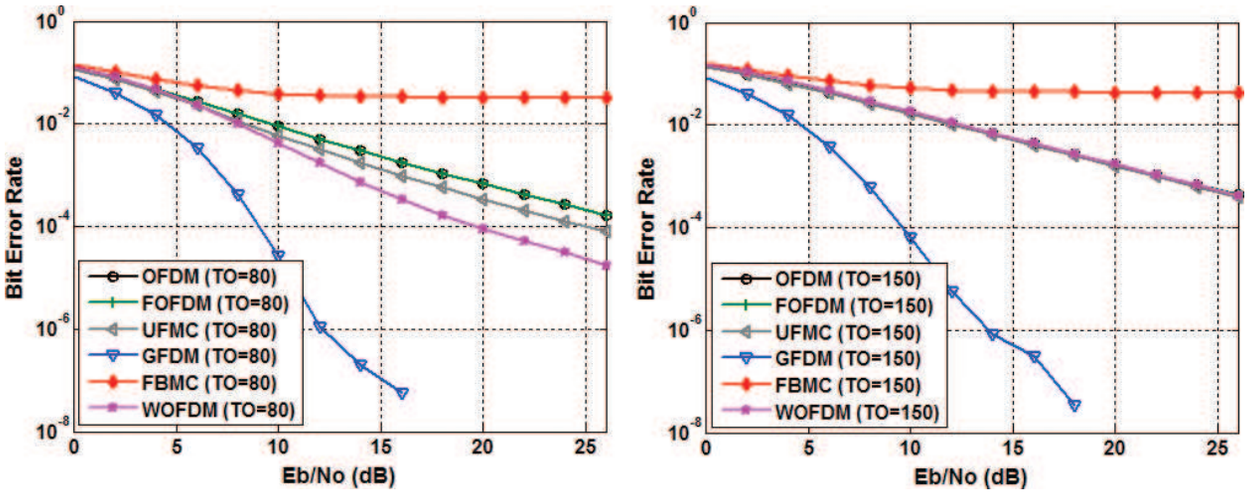

Figure 15. BER of QPSK/OQPSK in AWGN for TO = 80, 150 samples.

pilots [16], for channel estimation. Otherwise, the performance is severely degraded as can be seen in simulation results presented in **Figure 15** for TO = 80 and TO = 150 samples.

3.7. Computational complexity

The final figure of merit to be considered in this chapter is the computational complexity of different waveforms. In this section, computational complexity is evaluated in terms of number of real multiplications for each MCM Scheme. It is assumed that $N_u (N_u \leq N)$ subcarriers are loaded with transmitted symbols. A pair of N-point FFT and IFFT (via Split Radix FFT) with complexity $\mu_{FFT\&IFFT} = 2(N\log_2 N - 3N + 4)$ is used as the component in the efficient implementations of relevant MCM schemes.

Table 2 shows the computational complexity of the 5G candidate waveforms in terms of total number of required real multiplications per burst comprising of M multicarrier symbols (each MC symbol comprising of N subcarriers). While calculating complexity of UFMC and GFDM, it is assumed that each complex multiplication can be performed using three real multiplications. Complexity of OFDM comprises of IFFT and FFT complexity at the transmitter and receiver. FOFDM includes the added complexity due to transmit and receive filters. In FOFDM, it is assumed that the transmit filtering and adding CP could be combined such that the filtering is only performed once for the CP samples [12]. WOFDM has added complexity as compared to OFDM due to windowing that is a point wise multiplication operation. Complexity of UFMC transmitter is calculated based on number of real multiplication required for direct implementation of the operations given in **Figure 5**. Receiver complexity is derived based on the complexity of $2N$ point FFT operation performed at the UFMC receiver [2]. Complexity of FBMC is based on real multiplications required for filter, frequency shifting and FFT and IFFT operations in FBMC transceiver [10]. Complexity of GFDM is based on the low complexity transceiver architecture given in [7] in addition to the MN point FFT and IFFT operations required at the GFDM receiver to enable 1-tap FDE.

MCM	Number of real multiplications per burst	Normalized complexity
OFDM	$M\left(2(N\log_2 N - 3N + 4)\right)$	1
FOFDM	$M\left(2(N\log_2 N - 3N + 4) + 2NL + 2(N + N_{\text{CP}})L\right)$	4.8427
WOFDM	$M(2(N\log_2 N - 3N + 4) + 2(N + 0.25N))$	1.1785
UFMC	$M\left((2N\log_2 2N - 6N + 4) + \frac{N'}{D}(N\log_2 N - 3 + 4 + 2LN)\right)$	601.89
FBMC	$M\left(4(N\log_2 N - 3N + 4) + 4N + 8Np\right)$	5.7122
GFDM	$6MN\left(M + \log_2 N) + 2(MN\log_2 MN - 3MN + 4\right)$	11.8231

Table 2. Complexity of MCM schemes.

The last column of **Table 2** shows the complexity of each MCM scheme normalized to the OFDM complexity for $M = 14$, $N = 1024$, $D = 12$, $p = 6$, $N_{CP} = 72$, $N' = 664$, $L = 72$ (*UFMC*), and $L = 13$ (*FOFDM*). It is observed that as compared to OFDM, WOFDM has the lowest complexity. FOFDM and FBMC are approximately five and six times more complex than OFDM, while GFDM is nearly 12 times more complex as compared to OFDM. The highest complexity is shown by UFMC. The complexity of UFMC is directly proportional to the number of sub-bands which in turn depends on the sub-band size. It must be noted that more efficient ways of implementation, e.g. polyphase implementation given in [9], can reduce the complexity of UFMC by nearly 4.5 times. Using a smaller FFT size per sub-band in UFMC can also attain significant reduction in complexity

4. Summary

The waveforms for 5G networks should address certain challenges to meet the diverse set of requirements for future wireless communications. This chapter has described different candidate waveforms and some preliminary simulation results are presented to compare their performance with OFDM and verify the comparisons given in the literature summarized in **Table 3**. Based on the simulation results given in this chapter, performance of different waveforms as compared to OFDM is summarized in **Table 4**.

It is observed that while most of the results match the comparison found in the literature, TO and CFO resiliency of FBMC does not match the results in **Table 3** [15]. This is due to the fact that we have not taken into account any intrinsic interference cancellation techniques or FBMC-specific pilot design for improved channel estimation.

While 5G candidate waveforms show better spectral containment than OFDM making them suitable for carrier aggregation, other factors such as spectral efficiency, synchronization requirements and computational complexity need to be taken into account in order to find the most suitable techniques and corresponding tradeoffs for different 5G scenarios. However, this needs further simulations and analysis particularly in multi-user scenarios according to

Figure of merit	OFDM	FOFDM	WOFDM	FBMC	GFDM	UFMC
PAPR	High	High	High	High	Moderate (for SC-FDE)	High
OBE	High	Low	Low	Low	Low	Low
SE	Low	Low	Low	High	High	High
Computational complexity	Low	Moderate	Moderate	High	High	High
Short-burst traffic	No	No	No	No	Yes	Yes
Fragmented spectrum	No	No	Yes	Yes	Yes	Yes
TO resiliency	Poor	Poor	Moderate	Good	Good	Good
CFO resiliency	Poor	Poor	Moderate	Good	Good	Good

Table 3. Comparison of different MCM schemes [15].

Figure of merit	FOFDM	WOFDM	FBMC	GFDM	UFMC
PAPR	High	Similar	High	High	High
OBE	Low (in sidebands only) Similar (in fragments between available bands)	Low	Low	Slightly lowerLow (using guard symbols or windowing [2])	Low
Time-frequency efficiency	Similar	Low	High for longer bursts	High	High
Computational complexity	Moderate	Similar	Moderate	Moderate	High
Short-burst traffic	No	No	No	Yes	Yes
Fragmented spectrum	No	Yes	Yes	Yes	Yes
TO resiliency	Similar	Better	Poor	Better	Better
CFO resiliency	Similar	Lower	Poor	Better	Similar

Table 4. Summary of performance of different MCM schemes as compared to OFDM.

the propagation conditions of different 5G use cases and scenarios to understand the suitability of each candidate waveform in that specific environment.

Author details

Ayesha Ijaz*, Lei Zhang, Pei Xiao and Rahim Tafazolli

*Address all correspondence to: a.ijaz@surrey.ac.uk

Institute for Communication System (ICS), Home of 5G Innovation Centre (5GIC), University of Surrey, Guildford, UK

References

[1] Ijaz, A., et al. Enabling massive IoT in 5G and beyond systems: PHY radio frame design considerations. IEEE Access. 2016;**4**:3322–3339.

[2] 5GNOW deliverable D3.2_v1.3. 5G waveform candidate selection. 2014. Available at: http://www.5gnow.eu

[3] NGMN. 5G white paper. Available at: https://www.ngmn.org/uploads/media/NGMN_5G_White_Paper_V1_0.tif

[4] Xiao, P., Toal, C., Burns, D., Fusco, V., Cowan, C. Transmit and receive filter design for OFDM based WLAN systems. In: International Conference Wireless Communications and Signal Processing (WCSP); October 2010; IEEE; pp. 1–4.

[5] Bala, E., Li, J., Yang, R. Shaping spectral leakage: a novel low-complexity transceiver architecture for cognitive radio. IEEE Vehicular Technology Magazine. 2013;**8**(3):38–46.

[6] Siohan, P., Siclet, C., Lacaille, N. Analysis and design of OFDM/OQAM systems based on filterbank theory. IEEE Transactions on Signal Processing. 2002;**50**(5):1170–1183.

[7] Farhang, A., Marchetti, N., Doyle, L.E. Low complexity transceiver design for GFDM (forthcoming). arXiv:1501.02940.

[8] 5G: a technology vision. Huawei Technologies Co., Ltd.; 2013. Available at: https://www.scribd.com/document/251024709/5G-a-Technology-Vision

[9] Noguet, D., Gautier, M., Berg, V. Advances in opportunistic radio technologies for TVWS. EURASIP Journal on Wireless Communications and Networking. 2011;**2011**(1). DOI: 10.1186/1687-1499-2011-170.

[10] Du, J., Xiao, P., Wu, J., Chen, Q. Design of isotropic orthogonal transform algorithm-based multicarrier systems with blind channel estimation. IET Communications. 2012;**6**(16):2695–2704.

[11] Abdoli, M.J., Jia, M., Ma, J. Weighted circularly convolved filtering in OFDM/OQAM. In: IEEE 24th Annual International Symposium on Personal, Indoor, and Mobile Radio Communications (PIMRC); 8 September; 2013. pp. 657–661.

[12] Li, J., Bala, E., Yang, R. Resource block filtered-OFDM for future spectrally agile and power efficient systems. Physical Communication. 2014;**11**:36–55.

[13] 3GPP TS 36.104, Technical Specification Group Radio Access Network; Evolved Universal Terrestrial Radio Access (E-UTRA).Base Station (BS) radio transmission and reception, v8.2.0; May 2008.

[14] Schaich, F., Wild, T., Chen, Y. Waveform contenders for 5G-suitability for short packet and low latency transmissions. In: IEEE 79th Vehicular Technology Conference (VTC Spring); May 2014; pp. 1–5.

[15] Farhang, A., Marchetti, N., Figueiredo, F., Miranda, J.P. Massive MIMO and waveform design for 5th generation wireless communication systems. In: 1st International Conference on 5G for Ubiquitous Connectivity (5GU); November 2014; IEEE; pp. 70–75.

[16] Stitz, T., Ihalainen, T., Viholainen, A., Renfors, M. Pilot-based synchronization and equalization in filter bank multicarrier communications. EURASIP Journal on Advances in Signal Processing. 2010;(1). DOI: 10.1155/2010/741429.

IntechOpen

IntechOpen